Cell Reports

Supplemental Information

Premature Sister Chromatid Separation Is Poorly Detected by the Spindle Assembly Checkpoint as a Result of System-Level Feedback

Mihailo Mirkovic, Lukas H. Hutter, Béla Novák, and Raquel A. Oliveira

Figure S1

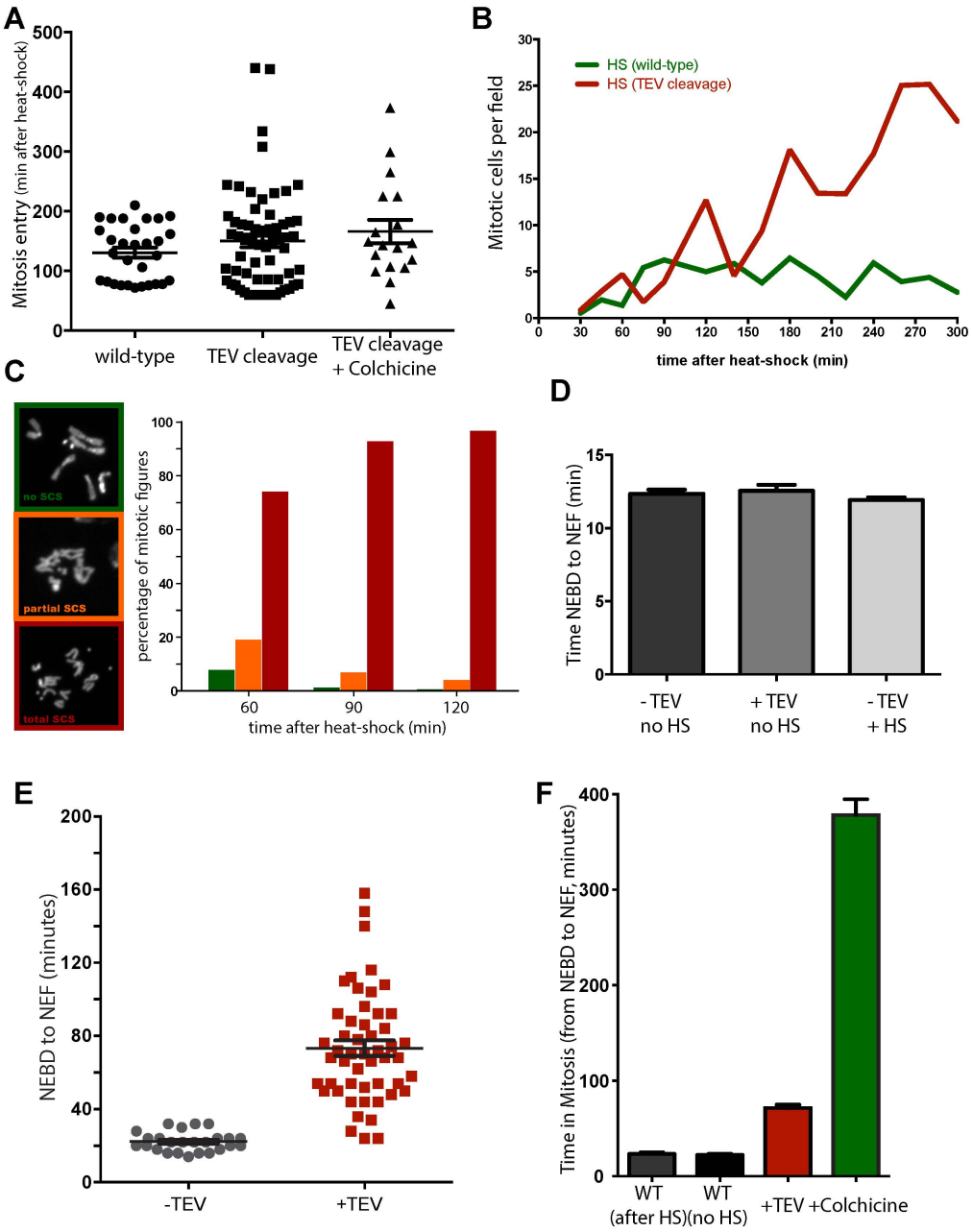

Figure S1, related to Figure 1 – TEV-mediated cleavage of cohesin allows analysis of the consequences of precocious sister chromatid cohesion separation within a single cell cycle. A) Time of entry into mitosis after heat-shock in the indicated experimental conditions showing that mitosis is not observed within the first 60 min after heat-shock, after which NBs asynchronously resume nuclear division. Note that TEV expression, cohesin cleavage or colchicine treatment, have no effect in the time of mitotic entry after heat-shock. **B)** Mitotic index in wild-type and cohesin-cleavage brains monitored in fixed samples at different times after heat-shock induced TEV expression; data points represent average number of mitotic figures (PH3 positive) per field. **C)** Quantification of precocious sister chromatid separation observed at different times after heat-shock-induced TEV protease expression, determined on acetic acid brain spreads (n=600 N=12 per time point, for each experimental condition); **D)** Time of mitosis (from NEBD to NEF) in the control without heatshock (n=62 N=6), control after heat-shock (n=41 N=4), and strains carrying the hsTEV transgene without heatshock (n=51 N=4), showing that neither heat-shock treatment nor leaky TEV expression influence progression through mitosis. **E)** Mitosis duration (NEBD to NEF) in heat-shocked wild-type and cohesin cleavage larval Ganglion Mother Cells (GMCs); **F)** Average mitosis duration (NEBD to NEF) in wild-type (n=20 N=3), wild-type after heat-shock, (n=25 N=3), cohesin cleaved (n=54 N=8), and colchicine treated (n=30 N=3) larval GMCs represented as mean ± SEM;

Figure S2

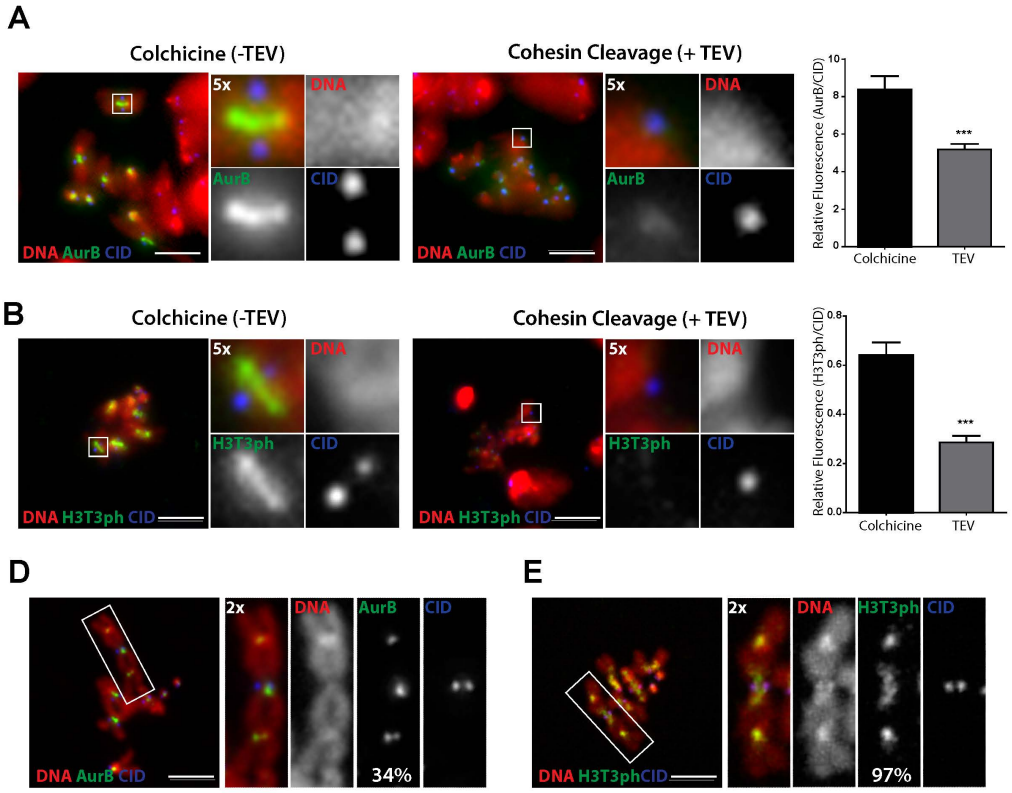

Figure S2, related to Figure 2 - Cohesin cleavage impairs proper centromeric localization of Aurora B. Spreads from larval brains from wild-type and cohesin cleaved strains immunostained for Aurora B **(A)** and H3T3ph **(B).** DNA is shown in red and CID in blue. Right graph depicts relative fluorescence intensity in the centromere vicinity in each experimental condition. **C)** Spreads from larval brains from C(2)EN strains immunostained for Aurora B (left) and H3T3ph (right) demonstrating their localization at ectopic heterochromatin sites, despite the absence of a proximal centromere (labelled with CID in blue). Numbers indicate the percentage of ectopic sites containing Aurora B / phH3T3. Scale bars are 5 µm.

Figure S3

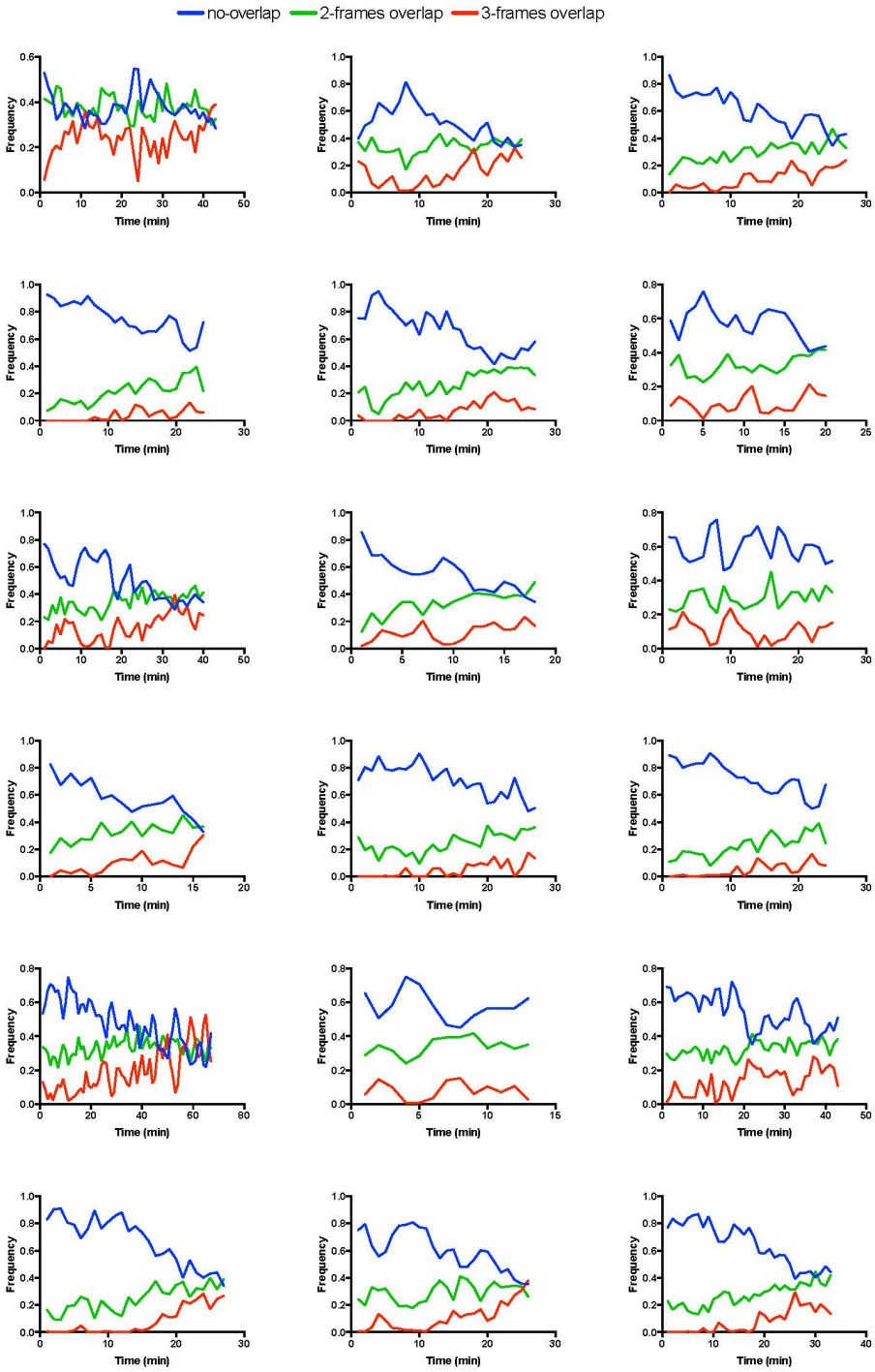

Figure S3, related to Figure 2 – Single chromatid movement decays gradually during mitotic delay induced by premature cohesin cleavage. Profile for chromatid movement observed in 18 individual cells after cohesin cleavage. Chromosome movement was measured from the displacement of individual centromeres within 3 consecutive frames, 6 min post-NEBD to anaphase onset; graphs represent frequency of overlapping pixels throughout the arrest. Blue represents non-overlapping pixels (fast movement), green represents pixels that overlap in 2 out of 3 frames (slow movement) and red represents pixels overlapping in the 3 frames (no movement). See also Movie S5.

Figure S4

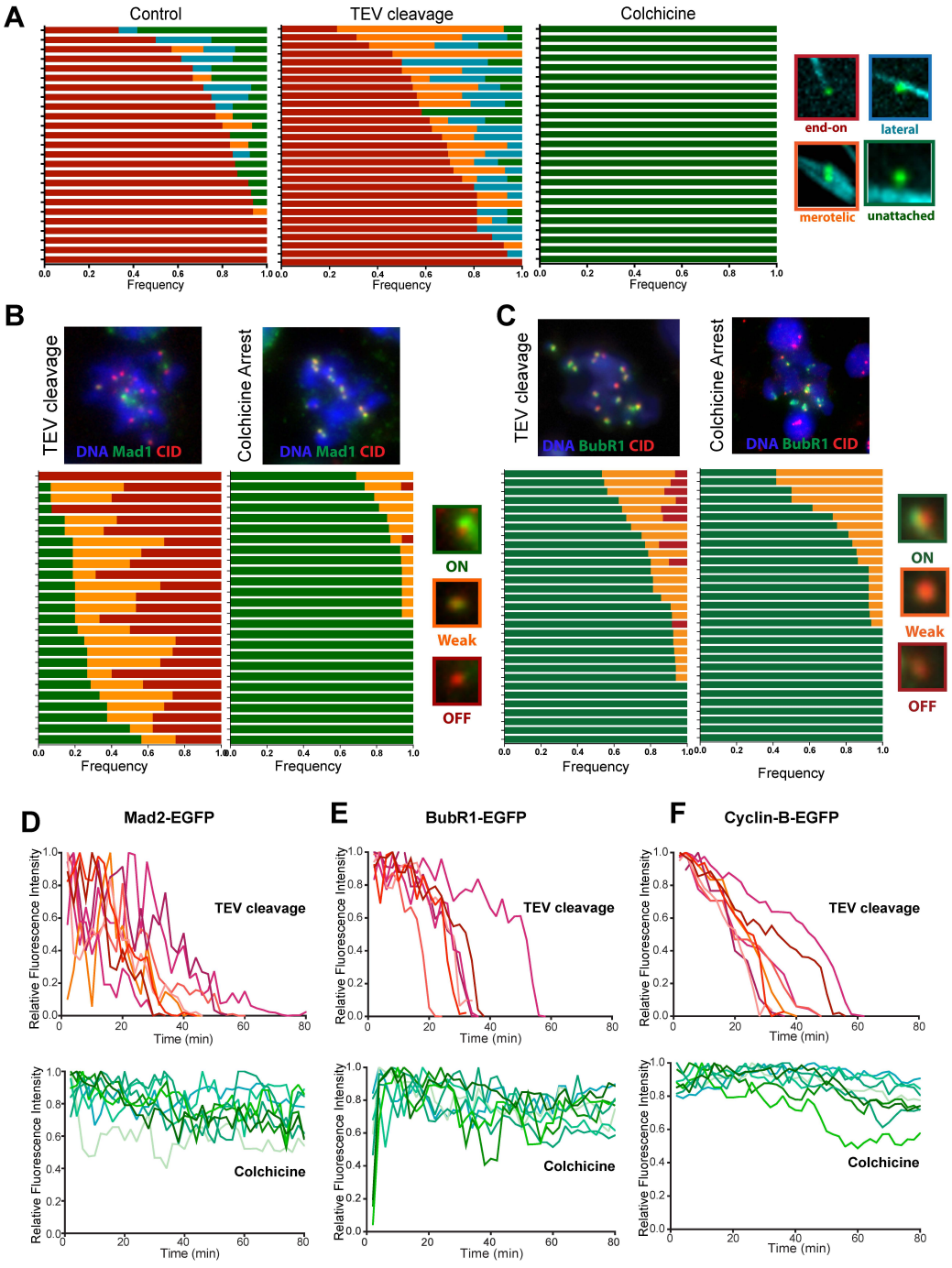

Figure S4, related to Figure 3 – Chromosome Attachment and localization of SAC components in single chromatids during mitotic arrest. A) Frequency of kinetochore attachment observed in controls (left), upon after cohesin cleavage (center) and after colchicine incubation (right); brains expressing HisH2Av-mRFP1 (red) and Cid-EGDP (green) were shortly incubated with 1:10.000 Sir-Tubulin probes (Cyan) before brain squash; each line in the graph represents the profile of a single cell (>25 NBs (N=3) for each experimental condition); **B and C)** Spreads from larval brains from colchicine-arrested and cohesin cleaved cells immunostained for Mad1 **(B)** and BubR1 **(C)** (in green). DNA is shown in blue and CID in red. Graph depicts relative frequency of kinetochores containing no, low, and high levels of Mad1/BubR1. Note that in contrast to colchicine-arrest, cohesin cleavage leads to reduced levels of Mad1 at kinetochores and a high asynchrony between the different analyzed cells (each at random points of the arrest). In contrast, BubR1 is mostly present at significant levels in all kinetochores of the analyzed cells. **(D-F)** Relative fluorescence intensity of Mad2-GFP **(D)**, BubR1-GFP **(E)** and CyclinB-GFP **(F)** in cohesin cleavage (red) and colchicine arrested (green) cells, normalized to the maximum value within each dataset. Times are relative to NEBD;

Figure S5

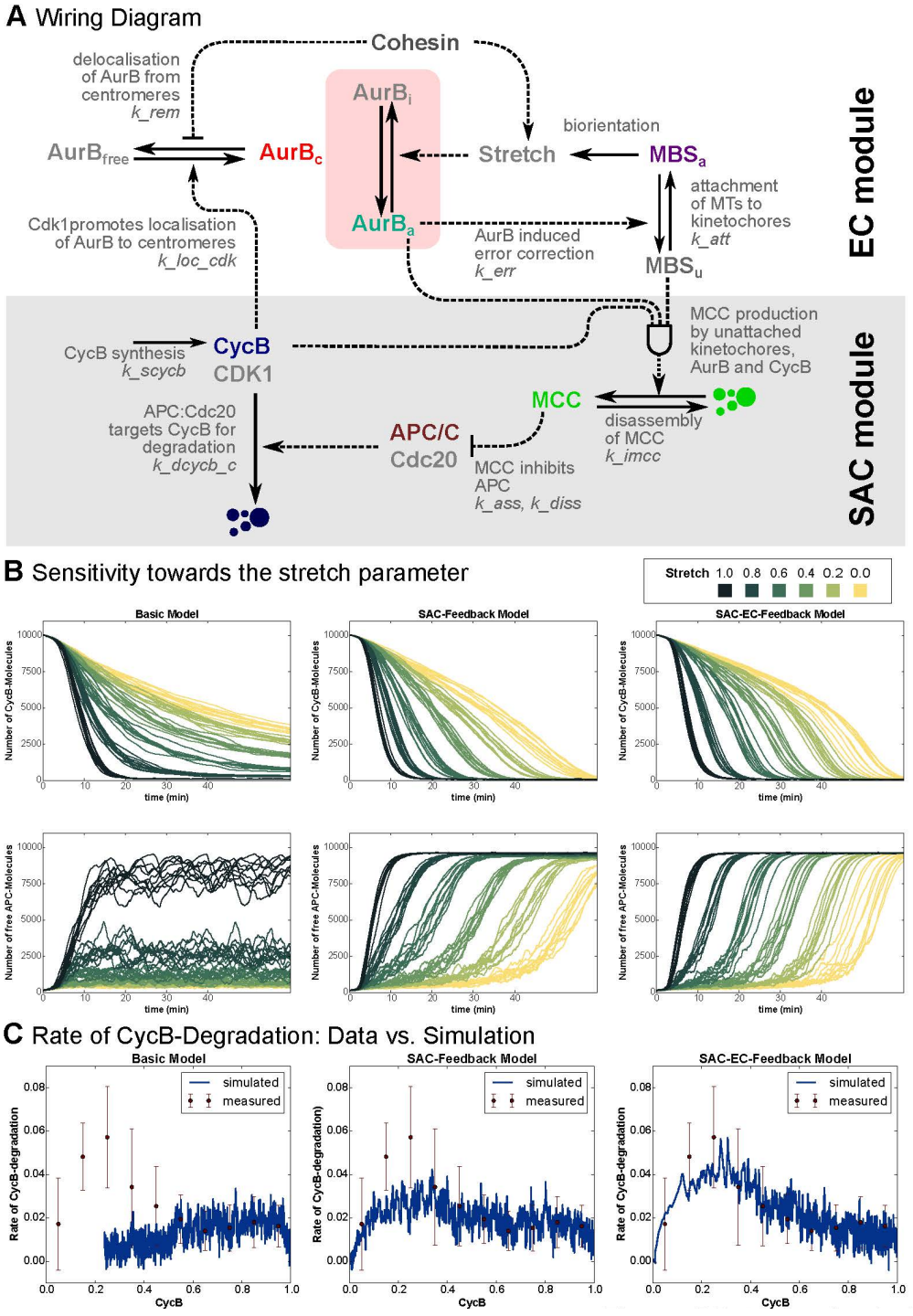

Figure S5, related to Figure 4 - Mathematical modelling of the interplay between error-correction (EC) and Spindle Assembly Checkpoint (SAC). A) Detailed molecular interaction network of EC and SAC: The EC module operates at centromeres/kinetochores and it uses Aurora-B activity to destabilize MT-KT attachments and thereby generates unattached MT-binding sites at KTs (MBSu) as an output of the EC module. Unattached MT binding sites of the KT signal to the SAC module by catalysing the production of Mitotic Checkpoint Complexes (MCC). MCC inhibition of APC/C-dependent CycB degradation regulates Cdk1 activity, which is the output of the SAC module. By promoting localization of AurB at centromeres, Cdk1 activity represents an input of EC. **B)** Numerical simulations of CycB (top row) and APC/C (bottom row) levels at different values of Stretch parameters in absence of cohesion with the three different models. **C)** Predicted rates of CycB-degradation after the loss of cohesins in the three model instances (blue lines) are plotted against degradation rates obtained from experimental data (red dots and error bars).

SUPPLEMENTAL MOVIES

Movie S1, related to Figure 1- Mitosis in a control neuroblast: Neuroblast undergoing mitosis after the heat shock. DNA is marked by H2AvD-mRFP1 (in red) centromere is marked by CID-GFP (in green). Times are relative to Nuclear Envelope Breakdown; scale bar equals 5 μm.

Movie S2, related to Figure 1 and 2- Nuclear division after cohesin cleavage: Neuroblast undergoing mitosis after cohesin has been cleaved prematurely by TEV; DNA is marked by H2AvD-mRFP1 (in red) centromere is marked by CID-GFP (in green); times are relative to Nuclear Envelope Breakdown). Note the dynamic behavior of centromeres upon premature cohesin cleavage; scale bar equals 5 μm.

Movie S3, related to Figure 2- Quantitative analysis of centromere motion after premature cohesin cleavage: Movies show walking average of the positions of centromeres (Cid-EGFP labelled) between 3 consecutive frames; Blue represents non-overlapping pixels, green represents pixels that overlap in 2 out of 3 frames and red represents pixels overlapping in the 3 frames. Movie shows 4 individual cells from 6 min-post NEBD until anaphase onset.

Movie S4, related to Figure 3- Kinetics of Mad2, BubR1 and Cyclin B upon cohesin cleavage: Time lapse imaging of Mad2-EGFP (left), BUBR1-GFP (middle), and Cyclin B-EGFP (right) in neuroblasts undergoing mitosis after cohesin cleavage by TEV protease. Times are relative to Nuclear Envelope Breakdown; scale bars are 5 μm.

SUPPLEMENTAL EXPERIMENTAL PROCEDURES

Fly strains:

To destroy cohesin by TEV protease cleavage, *Drosophila* strains were used with TEV-cleavable Rad21 ($Rad21^{TEV}$) in a Rad21-null background ($Rad21^{ex15}$, $Rad21^{550\text{-}3TEV}$-myc) (Pauli et al., 2008). TEV expression was induced by heat-shocking 3rd instar larvae at 37ºC for 45 minutes. After heat-shock, larvae were left to recover at room temperature. For live cell imaging, fly strains also expressed fluorescent markers as indicated in the tables below.

Table S1: List of Drosophila stocks used in this study.

Genotype	**Reference**
w-; +/+; Rad21^{ex15}, tubpr-Rad21$^{550\text{-}3TEV}$-myc *(4c)*	(Pauli et al., 2008)
w-; +/+; Rad21^{ex15}, poliubiq-His-RFP, tubpr-Rad21$^{550\text{-}3TEV}$ (4c)	(Oliveira et al., 2010)
w-; hspr-NLSv5TEV; Rad21^{ex3}/TM6B ubiGFP	(Pauli et al., 2008)
w-; HisH2AvD mRFP1 II.2; Cid-EGFP (CGC III.1)	(Schuh et al., 2007)
w-; HisH2AvD mRFP1 II.2 ; Rad21^{ex15}, tubpr-Rad21$^{550\text{-}3TEV}$(4c), CID-EGFP(CGC III.1)	(Oliveira et al., 2010)
w-; BubR1-GFP;+/+	(Buffin et al., 2005)
w- ; BubR1-GFP/CyO; Rad21^{ex15}, poliubiq-His-RFP, tubpr-Rad21$^{550\text{-}3TEV}$ (4c)	*This Study*
w- ; Mad2-GFP ; MKRS/TM6B	(Buffin et al., 2005)
w-; Mad2-GFP ; Rad21^{ex15}, poliubiq-His-RFP, tubpr-Rad21$^{550\text{-}3TEV}$(4c)	*This Study*
w-; poliubiq -CyclinB GFP	(Huang and Raff, 1999)
w-; poliubiq -CyclinB GFP ; Rad21^{ex15}, poliubiq-His-RFP, tubpr-Rad21 $^{550\text{-}3TEV}$(4c)	*This Study*
w+; C(2) EN;	(Novitski et al., 1981)

Table S2: List of specific genotypes used in this study.

Figure		**Label**	**Genotype**
1	A-C	-TEV	*w-; HisH2AvD mRFP1 II.2 ; Rad21^{ex15}, tubpr-Rad21$^{550\text{-}3TEV}$(4c), CID-EGFP(CGC III.1)*
		+TEV	*w-; hspr-NLSv5TEV/HisH2AvD-mRFP1 II.2; Rad21^{ex15}, tubpr-Rad21$^{550\text{-}3TEV}$*-myc *(4c), CID-EGFP-(CGCIII.1)/ Rad21^{ex3}*
		Colchicine	*w-; HisH2AvD mRFP1 II.2 ; Rad21^{ex15}, tubpr-Rad21$^{550\text{-}3TEV}$(4c), CID-EGFP(CGC III.1)*
2	A-E		*w-; hspr-NLSv5TEV/HisH2AvD-mRFP1 II.2; Rad21^{ex15}, tubpr-Rad21$^{550\text{-}3TEV}$*-myc *(4c), CID-EGFP-(CGCIII.1)/ Rad21^{ex3}*
3	A	Control	*w-; HisH2AvD mRFP1 II.2 ; Rad21^{ex15}, tubpr-Rad21$^{550\text{-}3TEV}$(4c), CID-EGFP(CGC III.1)*
		+ TEV	*w-; hspr-NLSv5TEV/HisH2AvD-mRFP1 II.2; Rad21^{ex15}, tubpr-Rad21$^{550\text{-}3TEV}$*-myc *(4c), CID-EGFP-(CGCIII.1)/ Rad21^{ex3}*
		Colchicine	*w-; HisH2AvD mRFP1 II.2 ; Rad21^{ex15}, tubpr-Rad21$^{550\text{-}3TEV}$(4c), CID-EGFP(CGC III.1)*
	B		*w-; hspr-NLSv5TEV/HisH2AvD-mRFP1 II.2; Rad21^{ex15}, tubpr-Rad21$^{550\text{-}3TEV}$*-myc *(4c), CID-EGFP-(CGCIII.1)/ Rad21^{ex3}*
	C	+TEV	*w-; hspr-NLSv5TEV/Mad2-EGFP; Rad21^{ex15}, poliubiq-His-RFP, tubpr-Rad21$^{550\text{-}3TEV}$(4c)/ Rad21^{ex3}*
	D	+TEV	*w-; hspr-NLSv5TEV/BubR1-EGFP; Rad21^{ex15}, poliubiq-His-RFP, tubpr-Rad21$^{550\text{-}3TEV}$(4c)/ Rad21^{ex3}*
	E	+TEV	*w-; hspr-NLSv5TEV/CycB-EGFP; Rad21^{ex15}, poliubiq-His-RFP, tubpr-Rad21$^{550\text{-}3TEV}$(4c)/ Rad21^{ex3}*
5	B, C		*w-; HisH2AvD mRFP1 II.2 ; Rad21^{ex15}, tubpr-Rad21$^{550\text{-}3TEV}$(4c), CID-EGFP(CGC III.1)*
	D	Control	*w-; HisH2AvD mRFP1 II.2 ; Rad21^{ex15}, tubpr-Rad21$^{550\text{-}3TEV}$(4c), CID-EGFP(CGC III.1)*
		+TEV	*w-; hspr-NLSv5TEV/Mad2-EGFP; Rad21^{ex15}, poliubiq-His-RFP, tubpr-Rad21$^{550\text{-}3TEV}$(4c)/ Rad21^{ex3}*
	F	+TEV	*w-; hspr-NLSv5TEV/Mad2-EGFP; Rad21^{ex15}, poliubiq-His-RFP, tubpr-Rad21$^{550\text{-}3TEV}$(4c)/ Rad21^{ex3}*
S1	A,D-F	-TEV	*w-; HisH2AvD mRFP1 II.2 ; Rad21^{ex15}, tubpr-Rad21$^{550\text{-}3TEV}$(4c), CID-EGFP(CGC III.1)*
		+TEV	*w; hspr-NLSv5TEV/HisH2AvD-mRFP1 II.2; Rad21^{ex15}, tubpr-Rad21$^{550\text{-}3TEV}$*-myc *(4c), CID-EGFP-(CGCIII.1)/ Rad21^{ex3}*
	B	-TEV	*w; +/+; Rad21^{ex15}, poliubiq-His-RFP, tubpr-Rad21$^{550\text{-}3TEV}$(4c)*
		+TEV	*w; hspr-NLSv5TEV/+; Rad21^{ex15}, poliubiq-His-RFP, tubpr-Rad21$^{550\text{-}3TEV}$(4c)/ Rad21^{ex3}*
	C		*w; hspr-NLSv5TEV/+; Rad21^{ex15}, poliubiq-His-RFP, tubpr-Rad21$^{550\text{-}3TEV}$(4c)/ Rad21^{ex3}*

S2	A,B	-TEV	*w; +/+; Rad21^{ex15}, poliubiq-His-RFP, tubpr-Rad21$^{550\text{-}3TEV}$(4c)*
		+TEV	*w; hspr-NLSv5TEV/+; Rad21^{ex15}, poliubiq-His-RFP, tubpr-Rad21$^{550\text{-}3TEV}$(4c)/ Rad21^{ex3}*
	C,D	C(2)EN	*w;C(2)EN, bw^{1},sp^{1};+/+*
S3			*w; hspr-NLSv5TEV/HisH2AvD-mRFP1 II.2; Rad21^{ex15}, tubpr-Rad21$^{550\text{-}3TEV}$*-myc *(4c), CID-EGFP-(CGCIII.1)/ Rad21^{ex3}*
S4	A	Control	*w-; HisH2AvD mRFP1 II.2 ; Rad21^{ex15}, tubpr-Rad21$^{550\text{-}3TEV}$(4c), CID-EGFP(CGC III.1)*
		+ TEV	*w-; hspr-NLSv5TEV/HisH2AvD-mRFP1 II.2; Rad21^{ex15}, tubpr-Rad21$^{550\text{-}3TEV}$*-myc *(4c), CID-EGFP-(CGCIII.1)/ Rad21^{ex3}*
		Colchicine	*w-; HisH2AvD mRFP1 II.2 ; Rad21^{ex15}, tubpr-Rad21$^{550\text{-}3TEV}$(4c), CID-EGFP(CGC III.1)*
	B, C	+ TEV	*w; +/+; Rad21^{ex15}, poliubiq-His-RFP, tubpr-Rad21$^{550\text{-}3TEV}$(4c)*
		Colchicine	*w; hspr-NLSv5TEV/+; Rad21^{ex15}, poliubiq-His-RFP, tubpr-Rad21$^{550\text{-}3TEV}$(4c)/ Rad21^{ex3}*
	D	+TEV	*w-; hspr-NLSv5TEV/Mad2-EGFP; Rad21^{ex15}, poliubiq-His-RFP, tubpr-Rad21$^{550\text{-}3TEV}$(4c)/ Rad21^{ex3}*
		Colchicine	*w-; Mad2-EGFP/CyO; Rad21^{ex15}, poliubiq-His-RFP, tubpr-Rad21$^{550\text{-}3TEV}$(4c)/TM6B*
	E	+TEV	*w-; hspr-NLSv5TEV/BubR1-EGFP; Rad21^{ex15}, poliubiq-His-RFP, tubpr-Rad21$^{550\text{-}3TEV}$(4c)/ Rad21^{ex3}*
		Colchicine	*w-; BubR1-EGFP/CyO; Rad21^{ex15}, poliubiq-His-RFP, tubpr-Rad21$^{550\text{-}3TEV}$(4c)/TM6B*
	F	+TEV	*w-; hspr-NLSv5TEV/CycB-EGFP; Rad21^{ex15}, poliubiq-His-RFP, tubpr-Rad21$^{550\text{-}3TEV}$(4c)/ Rad21^{ex3}*
		Colchicine	*w-; CycB-EGFP; Rad21^{ex15}, poliubiq-His-RFP, tubpr-Rad21$^{550\text{-}3TEV}$(4c)/TM3,Ser*

Brain Spreads and Immunofluorescence

DAPI spreads were performed by dissecting brains in 0.7% NaCl and incubated for 2 min in 45% acetic acid. Brains were transferred to a siliconized coverslip with 5 µl of 60% acetic acid for 30 seconds, squashed and transferred to liquid nitrogen. Slides were allowed to air dry before mounting in Vectashield mounting medium containing DAPI. For immunofluorescence, brains were dissected in 0.7% NaCl, incubated with 100 µM colchicine for one hour (when indicated), hypotonic shocked in 0.5% sodium citrate for 2–3 minutes, and fixed on a 5 µl drop of fixative (3.7% formaldehyde, 0.1% Triton-X100 in PBS) placed on top of a siliconized coverslip. After 30 seconds, the brains were squashed between the coverslip and a slide, allowed to fix for an additional 1 min and then placed in liquid nitrogen. Slides were further extracted with 0.1% Triton-X100 in PBS for 10 min, and proceded for immunofluorescence following standard protocols. Primary antibodies were rat anti-CID (Martins et al., 2009) used at 1:2000, rabbit anti-Mad1 used at 1:2000 (Conde et al., 2013), rabbit anti-BubR1 used at 1:2000 (Logarinho et al., 2004), anti-Aurora B rabbit used at 1:2000 (Adams et al., 2001), anti H3T3ph rabbit used at 1:1000 (Active Motif). Secondary antibodies conjugated with fluorescent dyes from Alexa series (Invitrogen) were used according to the manufacturer's instructions. All the fixed samples were observed with an inverted wide-field DeltaVision microscope (Applied Precision Inc.) equipped with a 10061.4 oil immersion objective (Olympus) and an EMCCD camera (Roper Cascade II or Roper Cascade 1024).

Tissue Preparation for live cell imaging

For live imaging brains were dissected 30 minutes after heat-shock in Schneider medium supplemented with 10% FBS (plus 100 µM Colchicine (Sigma), when indicated). Brains were mounted in 8 µl of medium in 35mm glass bottom dishes (MatTek), covered with an oxygen-permeable membrane (YSI membrane kit), and sealed with Voltalef 10S oil (VWR). This procedure allowed for long-term live imaging of 4-8 hours. For experiments that included drug addition during imaging acquisition (Binucleine 2 (Sigma-Aldrich) to a final

concentration of 25 µM and Roscovitine (Sigma-Aldrich) to the indicated final concentrations), brains were mounted in 200 µl of medium in the 35mm glass bottom dish coated by Concanavalin A. For characterization of the attachment profile upon cohesion depletion, brains were dissected in Schneider medium containing 10% FBS and 1:10 000 Sir Tubulin probe (Spirochrome). Given the low permeability of intact brains to the probe, the sample was cut into pieces and allowed to incubate for 30 minutes. Brains were subsequently squashed between the slide and a coverslip by capillary forces as previously described (Buffin et al., 2005). Time-lapse microscopy was performed with a spinning disk confocal microscope (Andor Revolution XD system) equipped with a 60xOil objective (Nikon, NA 1.4) and an Andor iXon 897 camera was used. All images were acquired by using a 20-26 µm thick imaging plane with 1 µm incremental z steps (except for chromosome attachment profiling where 0.2 was used). All images were assembled using ImageJ software (http://rsb.info.nih.gov/ij/) and selected stills were processed with Photoshop.

Measurements

All quantifications were performed using ImageJ software. Image z-stacks were projected (maximum projection) and background subtracted. For quantification of Aurora B and H3T3ph levels at the kinetochore, a fixed size ROI was used (1.6 x 0,5 µm in control chromosomes and 0.8 x 0,5 µm in single sisters). This ROI was placed between the kinetochore(s) and the centromeric signal and mean fluorescence intensity of AurB/H3T3Ph was normalized to corresponding CID. For measurements of kinetochore motion, CID-EGFP was imaged at 1-minute intervals. Images were segmented to select the centromere regions, based on a manual threshold (set 8 min post NEBD), to create binary images. For each movie, a walking average of 3 frames was produced (using kymograph plug-in, written by J. Rietdorf and A. Seitz, EMBL, Heidelberg, Germany) creating a merged image in which the intensity is proportional to the overlap between consecutive frames. Intensity profiles were used to estimate the percentage of non-overlaping, 2-frame overlap and 3-frame overlap pixels. Motion was quantified from the timeframe at which centromeres reached the poles (6-10 min post NEBD) until anaphase onset. Attachment profiles were scored based on CID-EFGP signal interactions with the microtubules labeled by SIR tubulin (1:10 000). Images were taken with a short z-distance (0,2 µm) and the attachment state of each kinetochore was scored in 3D by observing the entire z stack. Attachments were considered end-on if a single k-fiber was observed protruding from the centromere, lateral if the centromere was placed adjacently to a defined MT-fiber, merotelic if two fibers from opposite poles could be detected on a single centromere and unattached if CID-labelled centromeres were devoid of any MT fibers in their vicinity.

For measurement of Mad2, BubR1 and Cyclin B kinetics, brains were imaged in a 2 minutes interval (except for long-term CycB imaging were images were taken every 10 min). For analysis of Mad2 and BubR1 levels, a manual threshold was set to select the kinetochores 8 min after NEBD. Relative fluorescence was calculated by multiplying the area above the threshold by the mean fluorescence intensity, divided by the

maximal value within each dataset. For Cyclin B measurements, an ROI that comprises the entire NBs was used. Mean fluorescence intensities were measured at each time point and background subtracted (mean fluorescence intensity 4 minutes after anaphase onset). Relative fluorescence intensities were calculated by dividing by the maximum intensity within each data set.

Statistic analysis.

Statistical comparisons between sets of data were done using One-way or Two-way ANOVA (for multiple comparisons). All the statistic evaluation and graphic work was done in Graph Pad Prism 5. For each experimental set, “n” refers to the number of cells/kinetochores evaluated and “N” to the number of independent brains.

Mathematical modelling

The error-correction (EC) and Spindle Assembly Checkpoint (SAC) modules (Fig. 4) were converted into reaction-rate equations based on the following assumptions. The "Basic" and the "SAC-feedback" models are simplified versions of the "SAC-EC-feedback model", hence the description is based on the later and the changes to the simpler models are highlighted.

AurB molecules ($AurB_T$) are distributed between the centromeric form ($AurB_c$) and other cellular compartments ($AurB_T$ – $AurB_c$). In general, the models describe the localization of AurB at centromeres ($AurB_c$) as a combination of Cdk1:CycB-independent (k_{loc}) and -dependent (k_{loc_cdk}) processes. $AurB_c$ dissociation from centromeres follows first order kinetics with a rate constant of k_{rem} =2.5 min^{-1} and k_{rem} =10 min^{-1} in the presence and in the absence of cohesins, respectively:

$$\frac{d[AurB]_c}{dt} = \left(k_{loc} + k_{loc,cdk} \cdot [Cdk1]\right) \cdot ([AurB]_T - [AurB]_c) - k_{rem} \cdot [AurB]_c$$

The kinetic parameters of AurB localization are summarized below:

	"Basic model"	"SAC-feedback model"	"SAC-EC-feedback model"
k_{loc} (min^{-1})	3	3	0
$k_{loc,cdk}$ (min^{-1})	0	0	5

In case of Cdk1-driven localization ("SAC-EC-feedback model"), the steady state fraction of AurB at centromeres during prophase (Cdk1 = 1) is given by $\frac{[AurB]_c}{[AurB]_T} = \frac{k_{loc,cdk} \cdot [Cdk1]}{k_{loc,cdk} \cdot [Cdk1] + k_{rem}}$, which is 0.666 and 0.333 in the presence and in the absence of cohesins, respectively. We choose the total level of AurB 1.5 a.u., which sets the level of the centromeric pool ($AurB_c$) to 1 a.u. at the beginning of normal mitosis. Only a fraction of centromeric AurB ($AurB_a$) can destabilize MT-KT attachments at kinetochores (attached Microtubule Binding Sites - aMBS), because of kinetochore stretching caused by spindle tension. The rate of MT-KT attachments is proportional to MT-density (MT) and number of unattached MT binding sites at KTs (MBS_T - aMBS):

$$\frac{d[aMBS]}{dt} = k'_{att} \cdot [MT] \cdot ([MBS]_T - [aMBS]) - k_{err} \cdot \frac{[AurB]_a}{1 + [BN2]} \cdot [aMBS]$$

where [BN2] corresponds to the concentration of AurB inhibitor (binuclein2) relative to its IC_{50} value. Using 20-fold AurB inhibition ([BN2]=19) in the "SAC-EC-feedback model" reduces the length of TEV-induced mitosis (~45 mins) to about 9 mins (simulation not shown), consistent with our experiments on Fig. 2E.

The 'active' form of AurB ($AurB_a$) is reduced by MT-KT attachments (aMBS) according to a Hill-function (Ferrell and Ha, 2014), which approximates the cooperative effects among attached MT binding sites:

$$[AurB]_a = [AurB]_c \cdot \left(1 - Stretch \cdot \frac{[aMBS]^N}{J^N + [aMBS]^N}\right)$$

The value of Stretch parameter is one for chromosomes (Xs) and much smaller than one for individual sister-chromatids (SCs). Similar values were chosen for rate constants of MT-KT attachments (k_{att} =0.5 min^{-1}) and detachments (k_{err} =0.66 min^{-1}) which guarantees that saturating KTs with MT attachments requires AurB inactivation by the Stretch. In order to simulate the effect of spindle disruption by colchicine, MT should be set to zero.

The cellular level of APC/C is assumed to be constant (APC_T = 1 a.u.) during mitosis and distributed between active, free (APC) and MCC-bound, inactive (APC_T – APC) forms. The level of active APC is decreased by rapid MCC binding and increased by dissociation and disassembly of MCC (He et al., 2011):

$$\frac{d[APC]}{dt} = (k_{diss} + k_{imcc}) \cdot ([APC]_T - [APC]) - k_{ass} \cdot [APC] \cdot [MCC]_{free}$$

Association (k_{ass} = 200 min^{-1}) and dissociation (k_{diss} = 0.01 min^{-1}) rate constants are chosen to describe a tight binding of MMC and APC/C (Hein and Nilsson, 2014). The level of the limiting MCC component (labelled by MCC_T) is assumed to be in excess over APC/C (MCC_T =1.2 > APC_T), which is necessary requirement for stoichiometric inhibition (Verdugo et al., 2013). The assembled MCC could be associated with APC/C (APC_T – APC) or present in a free form (MCC_{free}). MCC_{free} is produced by unattached KTs from the pool of free MCC subunits at a rate proportional to the level of the limiting component (MCC_T – MCC_{free} - APC_T + APC). In the two models with SAC-feedbacks, the rate of production of MCC_{free} is proportional to both $AurB_a$ and Cdk1 activities, because these kinases activate checkpoint proteins at the kinetochore. The level of MCC_{free} is decreased by binding to APC/C (k_{ass}) and by disassembly of the complex (k_{imcc} = 0.5 min^{-1}) and it increased by dissociation from the MCC:APC complex (k_{diss}):

$$\frac{d[MCC]_{free}}{dt} = \left(k_{amcc} + k_{amcc,kin} \cdot \frac{[AurB]_a/(1+[BN2])}{J_{amc} + [AurB]_a/(1+[BN2])} \cdot [Cdk1]\right) \cdot [uMBS]$$
$$\cdot \left([MCC]_T - [MCC]_{free} - ([APC]_T - [APC])\right) - k_{ass} \cdot [APC] \cdot [MCC]_{free} + k_{diss}$$
$$\cdot ([APC]_T - [APC]) - k_{imcc} \cdot [MCC]_{free}$$

The kinetic parameters of MCC production are summarized below:

	"Basic model"	"SAC-feedback model"	"SAC-EC-feedback model"
k_{amcc} (min^{-1})	10	0	0
$k_{amcc\_,cdk}$ (min^{-1})	0	15	15

The low sensitivity of SAC to AurB inhibition (our data and (Santaguida et al., 2011)) suggests an efficient activation of SAC-proteins by AurB–kinase, which we describe with a hyperbolic ('saturating') function using a small 'saturation-constant' (J_{amc} = 0.1). Therefore after a 20-fold ([BN2]=19) inhibition the residual 5% activity of AurB-kinase could maintain a third of the MCC production rate. These parameter values reduce the length of colchicine-induced mitotic arrest, upon AuroraB inhibition, to about 60 mins (simulation not shown) in the "SAC-EC-feedback model", consistent with our experiments on Fig. 2E.

CycB is synthesized at a constant rate (k_{scycb}) and associates rapidly with Cdk1 present in excess, therefore the level of CycB determines Cdk1 activity via

$$[Cdk1] = \frac{[CycB]}{1 + [RO]}$$

where [RO] corresponds to the concentration of Cdk-inhibitor (roscovitine) relative to its IC_{50} value.

Cdk1 is inactivated by CycB degradation which has a small, APC/C-independent (k_{dcycb} = 0.004 min^{-1}, $t_{½}$ ≅ 170 min) and a large, APC/C-dependent rate constants ($k_{dcycb,apc}$ = 0.5 min^{-1} = $t_{½}$ ≅ 1.4 min):

$$\frac{d[CycB]}{dt} = k_{scycb} - \left(k_{dcycb} + k_{dcycb,apc} \cdot [APC]\right) \cdot [CycB]$$

The steady state level of CycB in the absence of APC/C activity (interphase) is k_{scycb}/k_{dcycb}, which we set to one by choosing the rate of CycB synthesis (k_{scycb}) identical to k_{dcycb} (= k_{scycb} = 0.004 min^{-1}).

The model was simulated by Gillespie's Stochastic Simulation Algorithm (SSA) after converting the rate of elementary reactions into propensity functions. We provide the code for stochastic simulation in the form of an ode-file for the freely available software XPPAut (http://www.math.pitt.edu/~bard/xpp/xpp.html).

To run the simulations in a programmatical manner, we used an scripting-interface for XPPAut (https://github.com/novakgroupoxford/XPPjl). The original code used to run and plot the simulations used in the figures is freely available at https://github.com/novakgroupoxford/2015_Mirkovic_et_al.

The initial conditions of numerical simulations are obtained from a steady state calculated without MT-binding to KTs (MT= 0) and lack of APC/C activity (k_{dcycb_apc} = 0), which corresponds to an interphase situation. The start of numerical simulations corresponds to nuclear envelope breakdown when the mitotic spindle starts to capture kinetochores and APC/C is activated by Cdk1:CycB, which is captured by setting [MT]= 1 and $k_{dcycb,apc}$ = 0.5 min^{-1}.

The stochastic simulation follows the number of molecules in a total volume (V_T) of 10^4 units. V_T is divided into a smaller (V_x) and a larger (V_{nx}) compartment in order to follow a single sister-kinetochore of a chromosome (normal mitosis)/sister-chromatid (TEV induced mitosis) and the collection of all the kinetochores within the cell, respectively. Since Drosophila somatic cells have 16 sister-kinetochores, the small volume is $V_x = V_T/16 = 625$ units while $V_{nx} = 15V_T/16 = 9375$. The components of the SAC (cytoplasmic) module are assumed to be more abundant than the EC (kinetochore/centromere) ones. Since we set the level of APC_T = 1and MCC_T = 1.2, these molecules are represented in the volume of 10^4 by 10^4 and $1.2 \cdot 10^4$ copies, respectively. The choice of $k_{scycb} = k_{dcycb}$ sets the initial number of CycB molecules to 10^4. Zero- and second-order rate-constants of the deterministic (concentration) models were scaled by volume and relative protein abundance.

We assume 11 microtubule-binding sites (MBS) on each sister-kinetochore (Maiato et al., 2006), which gives 176 binding sites on 16 sister-kinetochores, therefore we set the parameter MBS_{tot} = 0.0176. By choosing $AurB_T$ = 0.15 the total number of Aurora B molecules is $1.5 \cdot 10^3$, which are distributed between centromeric and free pools. At the beginning of mitosis, two-third (~10^3) and one-third (~500) AurB molecules are bound to centromeres in the presence and in the absence of cohesins, respectively (see above). These centromeric AurB molecules are distributed randomly among eight chromosomes and 16 sister-chromatids. Therefore on average ~60 (=1000/16) and ~30 (=500/16) AurB molecules are acting on a single sister-kinetochore in the presence and in the absence of cohesins, respectively.

```
##################################################
#
#      FULL STOCHASTIC MODEL FOR MIRKOVIC ET AL. 2015
#
##################################################

##################################################
#
#      VARIABLES
#
##################################################

# time for next reaction
tr'=tr-log(ran(1))/p14
uKT'=max(0,uKT+z1-z2)
APC'=max(1,APC+z3-z4)
MCCfree'=max(1,MCCfree+z5-z6)
CycB'=max(1,CycB+z7-z8)
AurBc'=max(0,AurBc+z9-z10)
uKTla'=max(0,uKTla+z11-z12)
AurBcla'=max(0,AurBcla+z13-z14)

##################################################
#
#      REACTION RATES
#
##################################################

# formation of unattached MT binding sites at the kinetochore of a single chromosome/sister-chromatid
V1 = kerr*AurBa/(1 + BN2)*(KTtot*Vx - uKT)/Vx
# formation of unattached MT binding sites at the kinetochore of a single chromosome/sister-chromatid
V2 = katt*uKT

# APC/C activation
V3 = (kdiss + kimcc)*(APCtot*VT - APC)
# APC/C inactivation
V4 = kass*APC*MCCfree/VT

# MCC production
V5 = (kamcc + kamcc_cdk/VT*Cdk1*AurBatot/(1 + BN2)/(Jamcc + AurBatot/(1 + BN2)))*(uKT + uKTla)*(MCCtot*VT - MCCfree - (APCtot*VT - APC))/VT + kdiss*(APCtot*VT
- APC)
# MCC inactivation
V6 = kimcc*MCCfree + kass*APC*MCCfree/VT

# CycB synthesis
V7 = kscycb*VT
# CycB degradation
V8 = (kdcycb + kdcycb_c*APC/VT)*CycB

# Aurora-B association with the centromere of a single chromsome/sister-chromatids
V9 = (kloc + kloc_cdk/VT*Cdk1)*(AurBtot*VT - AurBc - AurBcla)*Vx/VT
# Aurora-B dissociation form centromere of a single chromosome/sister-chromatids
V10 = krem*AurBc

# formation of unattached kinetochores of bulk chromosomes/sister-chromatids
V11 = kerr*AurBala/(1 + BN2)*(KTtot*Vbulk - uKTla)/Vbulk
# formation of attached kinetochores of bulk chromosomes/sister-chromatids
V12 = katt*uKTla

# Aurora-B association with the centromere of bulk chromsome/sister-chromatids
V13 = (kloc + kloc_cdk/VT*Cdk1)*(AurBtot*VT - AurBcla - AurBc)*Vbulk/VT
# Aurora-B dissociation form centromere of bulk chromosome/sister-chromatids
V14 = krem*AurBcla

##################################################
#
#      CUMULATIVE PROBABILITIES
#
##################################################

p1 = V1
p[2..14] = p[j-1] + V[j]

##################################################
#
#      CHOOSE REACTION
#
##################################################

s2 = ran(1)*p14
z1 = (s2<p1)
z[2..13]=(s2<p[j])&(s2>=p[j-1])
z14 = (s2>p13)
```

```
################################################
#
#      ALGEBRAIC EQUATIONS AND AUXILLIARY VARIABLES
#
################################################

AurBa=flr(AurBc*(1 - Stretch*(KTtot*Vx - uKT)^N/((J*KTtot*Vx)^N + (KTtot*Vx - uKT)^N)))
AurBala=flr(AurBcla*(1 - Stretch*(KTtot*Vbulk - uKTla)^N/((J*KTtot*Vbulk)^N + (KTtot*Vbulk- uKTla)^N)))
AurBatot=AurBa + AurBala
Cdk1=CycB/(1 + RO)
VT=Vx + Vbulk

aux uKTtot=uKT + uKTla
aux AurBa=AurBa
aux AurBctot=AurBc + AurBcla
aux AurBatot=AurBa + AurBala



################################################
#
#      INITIAL CONDITIONS
#
################################################

init tr=0
init uKT=11
init APC=117
init MCCfree=2128
init CycB=10052
init AurBc=62
init uKTla=165
init AurBcla=938

################################################
#
#      PARAMETERS
#
################################################

p Vx=625
p Vbulk=9375

p kass=200
p kdiss=0.01
p BN2=0
p RO=0
p kerr=6.66
p katt=0.5
p KTtot=0.0176
p N=4
p J=0.4
p Jamcc=50
p kamcc=0
p kamcc_cdk=750
p kimcc=0.5
p MCCtot=1.2
p kscycb=0.004
p kdcycb=0.004
p kdcycb_c=0.5
p kloc=0
p kloc_cdk=5
p krem=2.5
p Stretch=1
p APCtot=1
p AurBtot=0.15


################################################
#
#      NUMERICAL SETTINGS
#
################################################

@ bound=100000000
@ meth=discrete
@ total=2000000
@ njmp=1000
@ maxstorage=100000000
@ seed=189284124
done
```

SUPPLEMENTAL REFERENCES

Adams, R.R., Maiato, H., Earnshaw, W.C., and Carmena, M. (2001). Essential roles of Drosophila inner centromere protein (INCENP) and aurora B in histone H3 phosphorylation, metaphase chromosome alignment, kinetochore disjunction, and chromosome segregation. The Journal of cell biology *153*, 865-880.

Conde, C., Osswald, M., Barbosa, J., Moutinho-Santos, T., Pinheiro, D., Guimaraes, S., Matos, I., Maiato, H., and Sunkel, C.E. (2013). Drosophila Polo regulates the spindle assembly checkpoint through Mps1-dependent BubR1 phosphorylation. The EMBO journal *32*, 1761-1777.

Ferrell, J.E., Jr., and Ha, S.H. (2014). Ultrasensitivity part I: Michaelian responses and zero-order ultrasensitivity. Trends in biochemical sciences *39*, 496-503.

He, E., Kapuy, O., Oliveira, R.A., Uhlmann, F., Tyson, J.J., and Novak, B. (2011). System-level feedbacks make the anaphase switch irreversible. Proceedings of the National Academy of Sciences of the United States of America *108*, 10016-10021.

Hein, J.B., and Nilsson, J. (2014). Stable MCC binding to the APC/C is required for a functional spindle assembly checkpoint. EMBO reports *15*, 264-272.

Huang, J., and Raff, J.W. (1999). The disappearance of cyclin B at the end of mitosis is regulated spatially in Drosophila cells. The EMBO journal *18*, 2184-2195.

Maiato, H., Hergert, P.J., Moutinho-Pereira, S., Dong, Y., Vandenbeldt, K.J., Rieder, C.L., and McEwen, B.F. (2006). The ultrastructure of the kinetochore and kinetochore fiber in Drosophila somatic cells. Chromosoma *115*, 469-480.

Martins, T., Maia, A.F., Steffensen, S., and Sunkel, C.E. (2009). Sgt1, a co-chaperone of Hsp90 stabilizes Polo and is required for centrosome organization. The EMBO journal *28*, 234-247.

Novitski, E., Grace, D., and Strommen, C. (1981). The entire compound autosomes of Drosophila melanogaster. Genetics *98*, 257-273.

Schuh, M., Lehner, C.F., and Heidmann, S. (2007). Incorporation of Drosophila CID/CENP-A and CENP-C into Centromeres during Early Embryonic Anaphase. Current biology : CB *17*, 237-243.

Verdugo, A., Vinod, P.K., Tyson, J.J., and Novak, B. (2013). Molecular mechanisms creating bistable switches at cell cycle transitions. Open biology *3*, 120179.